Optics Letters

High-Q localized surface plasmon resonance based on bound states in the continuum for enhanced refractive index sensing

Haoran Chen,[1] Hongfei Wang,[2] Kwok-yin Wong,[2] and Dangyuan Lei[1,*]

[1]Department of Materials Science and Engineering, City University of Hong Kong, 83 Tat Chee Avenue, Kowloon, Hong Kong, China
[2]State Key Laboratory of Chemical Biology and Drug Discovery, Department of Applied Biology and Chemical Technology, The Hong Kong Polytechnic University, Hung Hom, Hong Kong, China
*Corresponding author: dangylei@cityu.edu.hk

Received 12 October 2021; revised 16 December 2021; accepted 16 December 2021; posted 16 December 2021; published 25 January 2022

Nanophotonics based on localized surface plasmon resonance (LSPR) has emerged as a vibrant arena for research into enhanced light–matter interactions with potential applications in imaging, sensing, and computing. However, the low quality (Q) factor of LSPR is a significant barrier to comprehensive device applications. Here, we demonstrate that coupling the LSPR of a gold nanowire array with the optical bound states in the continuum (BIC) of a dielectric double-layer grating can significantly increase the Q factor of LSPR. We realize two hybrid modes with Q factors of up to 111 at 558 nm and 83 at 582 nm, which are about 14 and 10 times larger than those of an uncoupled gold nanowire array. Based on temporal coupled-mode theory, we further show that the resonance frequencies and Q factors of the hybrid modes can be modulated and optimized by varying relevant structural parameters. This coupled system provides a new platform for improving the figures of merit (FoMs) of LSPR-based refractive index sensors, and the concept of LSPR–BIC coupling can be extended to other similar nanosystems.

https://doi.org/10.1364/OL.445453

Noble metal nanostructures can confine light into nanoscale spatial regions via the excitation of localized surface plasmon resonances (LSPRs), which enables a new realm of possibilities for many important applications in nanophotonics, such as surface-enhanced Raman scattering, sunlight harvesting, and biochemical sensing [1,2]. Nevertheless, due to the intrinsic absorption of metals and the large radiative scattering of metal nanostructures, the Q factor (defined as the energy dissipation per unit circle versus the energy stored in a resonator) of LSPR is usually much smaller than that of dielectric resonators [3–6]. Improving the Q factors of LSPRs is essential for the development of LSPR-based nanophotonic devices. Recently, several new design principles, including transformation optics [7–9], subgroup decomposition [10,11], and plasmon hybridization [12–17], have been proposed to suppress the radiative damping of LSPRs and thus increase their Q factors. In particular, coupling an individual metal nanostructure with a high-Q photonic microcavity to create a plasmonic-photonic hybrid system is an effective way to realize hybrid higher-Q resonances. For example, we have demonstrated a hybrid plasmonic-photonic system consisting of a metal nanoparticle in a dielectric Fabry–Perot (FP) microcavity, which shows a significantly reduced LSPR linewidth and consequently improved sensing performance [18]. However, the lossy Fabry–Perot cavity with a limited Q factor investigated in the earlier study requires optimization, and other frequently used high-Q modes built upon photonic crystal cavities and whispering-gallery microcavities are difficult to integrate due to their large dimensions (several tens of micrometers) [19–21]. Therefore, improving the Q factors of LSPRs or hybrid modes formed by LSPRs and other modes calls for new design concepts and approaches.

Recently, the optical bound states in the continuum (BICs) in dielectric micro- and nanostructures have attracted widespread attention in many research fields because their Q factors are theoretically predicted to be infinite. BICs are waves that remain localized even when they coexist within a continuous spectrum of radiation waves whose energy can leak away. Though defying conventional wisdom, BICs have been observed as general wave phenomena in different systems. In 1929, von Neumann and Wigner first proposed the possibility that localized eigenstates from the single-particle Schrodinger equation could be embedded in the continuum of leaky radiating modes [22]. Since then, many explanations for the formation mechanisms of BICs have been proposed, typically including destructive interference of resonances and mode symmetry incompatibility [23–28]. Recently, there have been numerous realizations of BICs in photonics, leading to a wide range of applications, such as lasers [29–31], sensors [32,33], filters [34,35], and low-loss fibers [36,37]. These studies provide possible means to realize narrower line widths and higher sensitivities of the abovementioned hybrid plasmonic-photonic devices.

Inspired by the recent theoretical prediction of BICs in a double-layer dielectric grating [38] and our earlier demonstration of the use of LSPR–FP coupling to effectively narrow the spectral linewidth of LSPR [18], we naturally wish to explore the possibility of combining dielectric BICs and metallic LSPRs to improve the Q factor of the latter. In this work, we propose a hybrid system comprising a metal nanowire array and a dielectric double-layer grating, where the broadband LSPR of the former

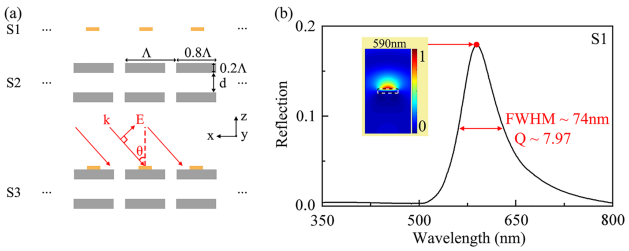

Fig. 1. (a) Schematic diagram of the coupled system (S3) consisting of a gold nanowire array (S1) and a dielectric double-layer grating (S2), where the gold nanowire array is placed at the surface of one grating layer such that their axes are in parallel along the y direction. (b) Simulated reflection spectrum of S1, showing an FWHM of 74 nm at a resonance wavelength 590 nm, corresponding to a quality factor of approximately 8. Inset shows the normalized magnetic field distribution profile at 590 nm.

can be effectively coupled with the BICs in the latter. Through theoretical analysis and parameter adjustment, the LSPR–BICs intermodal coupling can be analytically modeled and flexibly manipulated. We show that the LSPR Q factors for the gold nanowire array can be increased to 111 at a resonance wavelength of 558 nm and to 83 at 582 nm, which are about 14 and 10 times larger than those of the gold nanowire array in vacuum. In particular, by adjusting the distance between the two dielectric gratings in the coupled system, we can achieve effective modulation of the coupling strength and optimize the Q factors of the hybrid modes. Importantly, we demonstrate that the reported hybrid system can significantly improve the figure of merit (FoM) of a LSPR-based refractive index sensor (to about 100 at 558 nm and 67 at 582 nm).

As sketched in Fig. 1(a), the proposed hybrid system (S3) is composed of a one-dimensional (1D) gold nanowire array (S1) on a 1D double-layer dielectric grating (S2). The whole system is periodic in the x direction (the periodic constant is Λ) and infinite in the y direction. Each gold nanowire in S1 is 100 nm wide and 20 nm thick, and is seamlessly attached to one side of the bilayer grating in S3. Each dielectric slab in S2 is 0.8Λ wide and 0.2Λ thick, with the refractive index $n = 2$. In the z direction, the parameter d describes the distance between the two dielectric slabs. The hybrid system S3 can be analyzed by temporal coupled-mode theory (TCMT) [27], which is given by the 2×2 Hamiltonian matrix

$$H = \begin{pmatrix} \omega_1 & \kappa \\ \kappa & \omega_2 \end{pmatrix} - i \begin{pmatrix} \gamma_1 & \sqrt{\gamma_1\gamma_2}e^{i\psi} \\ \sqrt{\gamma_1\gamma_2}e^{i\psi} & \gamma_2 \end{pmatrix}, \quad (1)$$

where ω_1 (ω_2) and γ_1 (γ_2) are the eigenfrequency and radiation rate of a single-layer grating without (with) a gold nanowire array, respectively. The parameter κ is the near-field coupling strength between the two grating layers, and $\psi = k_z d$ is the phase shift of propagation between the two grating layers, where k_z is the propagation wavenumber along the z direction, which depends on the frequency and the angle of incidence θ. The eigenstates of the coupled system can be obtained by diagonalizing the above matrix. The two eigenfrequencies of H are

$$\omega_\pm = \frac{\omega_1+\omega_2}{2} - i\frac{\gamma_1+\gamma_2}{2} \pm \sqrt{\frac{[\omega_1-\omega_2-i(\gamma_1-\gamma_2)]^2}{4} + \left(\kappa - i\sqrt{\gamma_1\gamma_2}e^{i\psi}\right)^2}. \quad (2)$$

For the dielectric double-layer grating system (S2), when the two layers have no inter-layer coupling (i.e., d is very large), they share the same eigenfrequency $\omega_0 = \omega_1 = \omega_2$ and the same radiation rate $\gamma_0 = \gamma_1 = \gamma_2$. When the inter-layer coupling is significant (i.e., d is very small), Eq. (2) shows that the eigenvalues of S2 are $\omega_\pm = \omega_0 \pm \kappa - i\gamma_0(1 \pm e^{i\psi})$. When the round-trip phase shift 2ψ is an integer multiple of 2π, i.e., $k_z d = n\pi$, $n \in \mathbb{Z}$, one of the two eigenvalues turns into a BIC without an imaginary part, and the other eigenvalue becomes more lossy, with twice the original radiation rate. According to the definition of the Q factor, $Q_\pm = Re[\omega_\pm]/2\mathrm{Im}[\omega_\pm]$, the mode without an imaginary part has an infinite Q factor in theory. This is the so-called Fabry–Perot-type BIC mode, which can be obtained by tuning the structural parameters of S2, such as Λ and d. Due to the large intrinsic loss of gold in the gold nanowire array system (S3), the radiation rate γ_2 of the grating layer attached to the gold nanowire array is much larger than the radiation rate γ_1 of the grating layer beneath. The unreducible variables in Eq. (2), such as $\gamma_{1,2}$, $\omega_{1,2}$, κ, and ψ, make it difficult to maximize the Q factor of the hybrid system analytically. Nevertheless, by setting the two grating eigenfrequencies of S2 to be equal to the LSPR frequency of S1, i.e., $\omega_1 = \omega_2$, the solution of the hybrid system (S3) in Eq. (2) can be simplified to $\omega_\pm = \frac{\omega_1+\omega_2}{2} - i\frac{\gamma_1+\gamma_2}{2} \pm \sqrt{-\frac{(\gamma_1-\gamma_2)^2}{4} + \left(\kappa - i\sqrt{\gamma_1\gamma_2}e^{i\psi}\right)^2}$, where the Q factors depend mainly on k_z and d. By combining the TCMT-based analysis and numerical calculations, we can optimize the hybrid system and realize hybrid LSPR–BICs modes with improved Q factors.

In this study, the spectral properties of the three systems are calculated by the rigorous coupled-wave analysis (RCWA) method. RCWA is a frequency-domain modal method that decomposes the dielectric permittivity function of the grating and the electromagnetic fields in the plane of the grating in terms of their Fourier series expansions. The reflectance amplitude can be obtained by enforcing the boundary conditions at the interfaces between different layers. RCWA has been widely used for analyzing periodic optical structures because of its accurate far-field calculations and fast convergence.

As shown in Fig. 1(b), the LSPR peak of the gold nanowire array in vacuum is located at about 590 nm, with a FWHM of about 74 nm, corresponding to a Q factor of approximately 8.0. In order to obtain a Fabry–Perot-type BIC with an ultra-high Q factor as mentioned above, we first study the scattering properties of the dielectric double-layer grating system without the gold nanowire array [i.e., S2 in Fig. 1(a)]. Here, the grating period Λ is set at 450 nm, and the distance between two grating layers d is set as $0.65\Lambda = 292.5$ nm. Figure 2(a) exhibits the simulated overall specular reflection coefficient as a function of wavelength and angle of incidence θ. The bright regions in the map present sharp resonance modes corresponding to the trapped electromagnetic states in the grating. To further visualize the resonance features, Fig. 2(b) presents the reflectance spectra at three incident angles [indicated by the labels (1)–(3) in Fig. 2(a)], namely 8°, 11.5°, and 15°. All three spectra show three resonance peaks at around 425 and 560 nm. Importantly, comparison of the three spectral regions shown in the inserts of Fig. 2(b) reveals that the low-frequency resonance peak at 580.5 nm in the reflection spectrum obtained at an incidence of 11.5° disappears; this corresponds to a BIC with almost no leakage. As shown in the inserts of Fig. 2(a), the existence of the BIC mode is confirmed by the extreme near-field confinement in comparison with the leaky mode at 559 nm in the spectrum

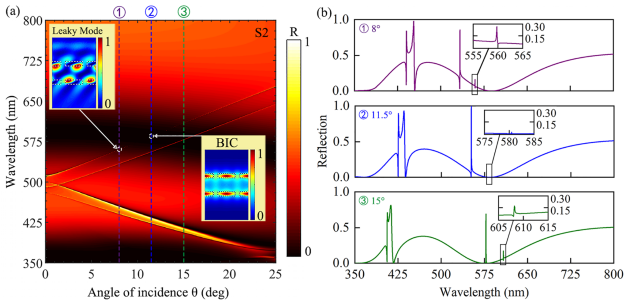

Fig. 2. Scattering properties of the dielectric double-layer grating system (S2). (a) Contour plot of the calculated specular reflection coefficient as a function of wavelength and the angle of incidence (θ). Insets are the normalized magnetic field distributions at 559 nm for an 8° angle of incidence (top left) and at 580.5 nm for an 11.5° angle of incidence (bottom right). (b) Simulated specular reflection coefficient as a function of wavelength for three incident angles ($\theta = 8°$, 11.5°, 15°) as labeled in (a), with the insets showing the spectral features of the low-frequency resonance mode. The disappearance of the low-frequency resonance peak at an incident angle of 11.5° indicates a trapping mode without radiation leakage.

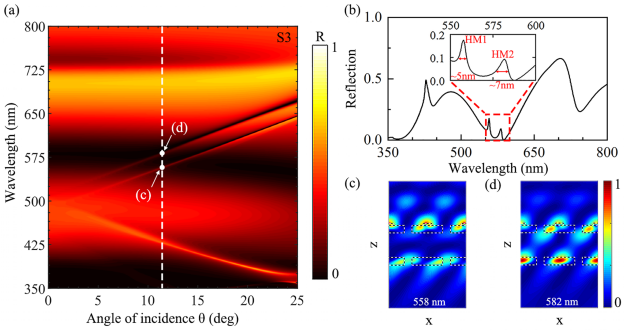

Fig. 3. Scattering properties of the hybrid system (S3). (a) Contour plot of the calculated specular reflection coefficient as a function of the wavelength and angle (θ) of the incident light. (b) Simulated specular reflection coefficient as a function of the wavelength at an incident angle of θ = 11.5°, as labeled in (a), with the inset showing the spectral features of the two hybrid resonance modes. The first (second) hybrid mode HM1 (HM2) is located at 558 nm (582 nm), with a FWHM of 5 nm (7 nm), corresponding to a Q factor of approximately 111 (83). (c), (d) Normalized magnetic field distributions for HM1 and HM2, respectively.

obtained at 8° incidence. The linewidth of this BIC is close to zero, meaning that the corresponding spectrum merges into the background. In general, the resonance wavelengths and Q factors of BIC or quasi-BIC modes can be adjusted by tuning structural parameters, which provides an easy-to-implement method to realize multifunctional systems.

We then investigate the scattering properties of the hybrid system [i.e., S3 in Fig. 1(a)]. Figure 3(a) shows the simulated overall specular reflection coefficient as a function of wavelength and angle of incidence θ. Three bright branches of resonance modes appear at positions similar to those in Fig. 2(a), including one below 500 nm and two above 500 nm. The darkest regions of these branches correspond to two hybrid modes with extremely high Q factors, which are labeled with white dots in Fig. 3(a). To visualize the spectral features of these hybrid modes, Fig. 3(b) shows the reflectance spectra for an incident angle θ = 11.5°, indicated by the dashed line in Fig. 3(a). In particular, two hybrid modes [HM1 and HM2, as shown in the insert of Fig. 2(b)] occur at a wavelength similar to the BIC in the S2 case. The FWHMs of HM1 and HM2 are reduced to about 5 and 7 nm, leading to Q factors of 111 and 83, which are about 14 and 10 times larger than those of the LSPR in the gold nanowire array (S1). Figures 3(c) and 3(d) show the normalized magnetic field distributions for HM1 and HM2, both of which exhibit a significant hybridization feature where the electromagnetic field appears not only in the dielectric grating but also at the surface of the metal nanowire array. Note that the field profile of HM1 is dominant in the upper grating layer, while the field profile of HM2 is dominant in the underneath layer, revealing distinctive contributions from the LSPR and grating modes to different hybrid modes.

In order to optimize the Q factors of the hybrid system, we explore how the HM1 and HM2 modes evolve with d in this hybrid system. Figure 4(a) shows the overall specular reflection coefficient as a function of the incident wavelength and d (ranging from 0 to 3Λ) at an angle of incidence θ = 11.5°. The bright lower (HM1) and upper (HM2) branches are distinguishable for small d but gradually degenerate with increasing d. As shown in Fig. 4(b), the resonance wavelength of HM1 decreases with increasing d while that of HM2 increases, leading to a smaller and smaller difference between them. Here, the resonance frequencies of HM1 and HM2 correspond to the two eigenvalues of the Hamiltonian given in Eq. (2). Since the near-field coupling strength κ is negatively correlated with d, the evolution of the two eigenfrequencies in Eq. (2) is consistent with the above simulation results. We also display the FWHMs and Q factors of HM1 and HM2, which vary with d, in Fig. 4(c). By solely adjusting d, we can modulate the κ of the hybrid system to optimize the Q factors; simulation results show that the hybrid system has its maximum Q factors at $d = 0.65\Lambda$. As a result, the Q factors of the hybrid system can be optimized to 111 for HM1 and 83 for HM2, about 14 and 10 times larger than those of the gold nanowire array in vacuum.

Due to their broad LSPR profiles, the optical spectrum of a Au nanowire array generally exhibits only slight changes according to the refractive index of its environment [39,40]. Here, the hybrid system provides strong coupling between the LSPR and BICs, and the BICs significantly prolong the interaction of the Au nanowires with light, thus enhancing the overall sensitivity of refractive-index sensing. Figure 5 shows how the reflection spectrum of the hybrid system changes as the background refractive index is increased from 1.00 to 1.03. The peak at 558 nm

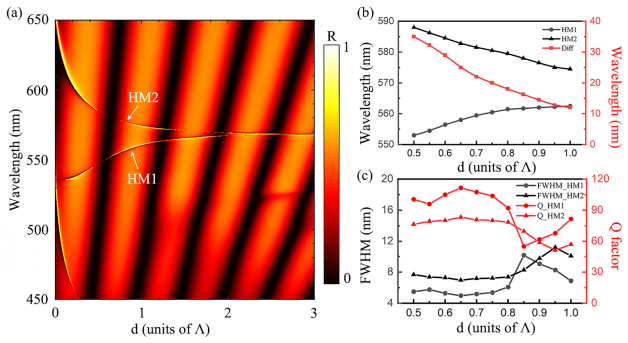

Fig. 4. (a) Contour plot of the specular reflection coefficient for the hybrid system S3, obtained by sweeping the incident wavelength and d at an angle of incidence θ of 11.5°. (b) Resonance wavelengths of HM1 and HM2 (left y axis) and the difference between them (right y axis) as a function of d extracted from (a). (c) FWHMs (left y axis) and Q factors (right y axis) of HM1 and HM2 as a function of d extracted from (a).

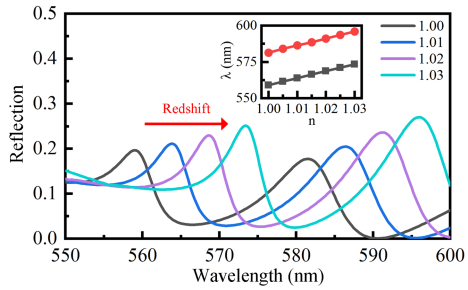

Fig. 5. Simulated reflection spectra of two hybrid systems exposed to environments with different refractive indices. The inset plots their resonant wavelength shifts. Left to right 1.00, 1.01, 1.02, 1.03.

(582 nm) shows a monotonous redshift to 573 nm (596 nm). As shown in the inset, the wavelength shift (λ_{shift}) of HM1 (HM2) is 15 nm (14 nm). Thus, the calculated FoM (defined as FoM = $\left(\frac{\lambda_{\text{shift}}}{\Delta n}\right)$ /FWHM in [40]) is about 100 at 558 nm and 67 at 582 nm, respectively, much larger than those obtained for other typical metal nanostructure-based LSPR sensors [18,41–43].

In summary, we have proposed a hybrid system comprising a metal nanowire array and a dielectric double-layer grating, where the broadband LSPR of the former can be coupled with the BICs of the latter to improve the LSPR Q factor. Through TCMT-based theoretical analysis and parameter scanning, the LSPR-BIC intermodal coupling can be analytically modeled and flexibly manipulated. Numerical simulation results confirm that this coupling can effectively suppress the radiative damping of the LSPR and thus significantly increase the LSPR Q factor 14-fold at the resonance wavelength of 558 nm and 10-fold at 582 nm. We have shown that solely adjusting the distance between the two dielectric grating layers in the hybrid system allows for effective modulation of the Q factors. Importantly, we have demonstrated that this hybrid system can efficiently improve the FoM of a LSPR-based refractive index sensor (to about 100 at 558 nm and 67 at 582 nm). The LSPR–BICs coupling concept can be generalized to other plasmonic structures to enhance their Q factors, allowing stronger light–matter interactions to be realized in various nanophotonic devices, such as sensors, filters, lasers, and nonlinear optics.

Funding. Hong Kong Polytechnic University (K-BBX4); City University of Hong Kong (9610456); University Grants Committee (C6013-18G).

Disclosures. The authors declare no conflicts of interest.

Data availability. Data underlying the results presented in this Letter are not publicly available at this time but may be obtained from the authors upon reasonable request.

REFERENCES

1. F. Favier, E. C. Walter, M. P. Zach, T. Benter, and R. M. Penner, Science **293**, 2227 (2001).
2. C. Wadell, S. Syrenova, and C. Langhammer, ACS Nano **8**, 11925 (2014).
3. T. Shegai and C. Langhammer, Adv. Mater. **23**, 4409 (2011).
4. A. Yang, M. D. Huntington, M. F. Cardinal, S. S. Masango, R. P. Van Duyne, and T. W. Odom, ACS Nano **8**, 7639 (2014).
5. C. Wadell, F. A. A. Nugroho, E. Lidström, B. Iandolo, J. B. Wagner, and C. Langhammer, Nano Lett. **15**, 3563 (2015).
6. N. Liu, M. L. Tang, M. Hentschel, H. Giessen, and A. P. Alivisatos, Nat. Mater. **10**, 631 (2011).
7. A. Aubry, D. Y. Lei, S. A. Maier, and J. B. Pendry, Phys. Rev. Lett. **105**, 233901 (2010).
8. P. West, S. Ishii, G. Naik, N. Emani, V. Shalaev, and A. Boltasseva, Laser Photonics Rev. **4**, 795 (2010).
9. J. B. Pendry, A. Aubry, D. R. Smith, and S. A. Maier, Science **337**, 549 (2012).
10. J. B. Lassiter, H. Sobhani, M. W. Knight, W. S. Mielczarek, P. Nordlander, and N. J. Halas, Nano Lett. **12**, 1058 (2012).
11. M. Rahmani, D. Y. Lei, V. Giannini, B. Lukiyanchuk, M. Ranjbar, T. Y. F. Liew, M. Hong, and S. A. Maier, Nano Lett. **12**, 2101 (2012).
12. E. Prodan, C. Radloff, N. J. Halas, and P. Nordlander, Science **302**, 419 (2003).
13. Q. Le-Van, E. Zoethout, E.-J. Geluk, M. Ramezani, M. Berghuis, and J. Gómez Rivas, Adv. Opt. Mater. **7**, 1801451 (2019).
14. Z. Sekkat, S. Hayashi, D. V. Nesterenko, A. Rahmouni, S. Refki, H. Ishitobi, Y. Inouye, and S. Kawata, Opt. Express **24**, 20080 (2016).
15. S. Hayashi, D. V. Nesterenko, and Z. Sekkat, Appl. Phys. Express **8**, 022201 (2015).
16. S. Hayashi, D. V. Nesterenko, and A. Z. Sekkat, J. Phys. D: Appl. Phys. **48**, 325303 (2015).
17. P. Wang, Y. Wang, Z. Yang, X. Guo, X. Lin, X.-C. Yu, Y.-F. Xiao, W. Fang, L. Zhang, G. Lu, Q. Gong, and L. Tong, Nano Lett. **15**, 7581 (2015).
18. M. A. Schmidt, D. Y. Lei, L. Wondraczek, V. Nazabal, and S. A. Maier, Nat. Commun. **3**, 1108 (2012).
19. K. J. Vahala, Nature **424**, 839 (2003).
20. D. Chanda, K. Shigeta, T. Truong, E. Lui, A. Mihi, M. Schulmerich, P. V. Braun, R. Bhargava, and J. A. Rogers, Nat. Commun. **2**, 479 (2011).
21. F. Gu, L. Zhang, Y. Zhu, and H. Zeng, Laser Photonics Rev. **9**, 682 (2015).
22. U. Fano, Phys. Rev. **124**, 1866 (1961).
23. J. Lee, B. Zhen, S. L. Chua, W. Qiu, J. D. Joannopoulos, M. Soljačić, and O. Shapira, Phys. Rev. Lett. **109**, 067401 (2012).
24. C. W. Hsu, B. Zhen, J. Lee, S. L. Chua, S. G. Johnson, J. D. Joannopoulos, and M. Soljačić, Nature **499**, 188 (2013).
25. S. Longhi and G. Della Valle, Sci. Rep. **3**, 2219 (2013).
26. A. Kodigala, T. Lepetit, Q. Gu, B. Bahari, Y. Fainman, and B. Kanté, Nature **541**, 196 (2017).
27. C. W. Hsu, B. Zhen, A. D. Stone, J. D. Joannopoulos, and M. Soljacic, Nat. Rev. Mater. **1**, 16048 (2016).
28. H. F. Wang, S. K. Gupta, X. Y. Zhu, M. H. Lu, X. P. Liu, and Y. F. Chen, Phys. Rev. B **98**, 214101 (2018).
29. H. Matsubara, S. Yoshimoto, H. Saito, Y. Jianglin, Y. Tanaka, and S. Noda, Science **319**, 445 (2008).
30. K. Hirose, Y. Liang, Y. Kurosaka, A. Watanabe, T. Sugiyama, and S. Noda, Nat. Photonics **8**, 406 (2014).
31. C. Huang, C. Zhang, S. Xiao, Y. Wang, Y. Fan, Y. Liu, N. Zhang, G. Qu, H. Ji, J. Han, L. Ge, Y. Kivshar, and Q. Song, Science **367**, 1018 (2020).
32. A. A. Yanik, A. E. Cetin, M. Huang, A. Artar, S. H. Mousavi, A. Khanikaev, J. H. Connor, G. Shvets, and H. Altug, Proc. Natl. Acad. Sci. U. S. A. **108**, 11784 (2011).
33. B. Zhen, S. L. Chua, J. Lee, A. W. Rodriguez, X. Liang, S. G. Johnson, J. D. Joannopoulos, M. Soljačić, and O. Shapira, Proc. Natl. Acad. Sci. U. S. A. **110**, 13711 (2013).
34. J. M. Foley, S. M. Young, and J. D. Phillips, Phys. Rev. B **89**, 165111 (2014).
35. L. L. Doskolovich, E. A. Bezus, and D. A. Bykov, Photonics Res. **7**, 1314 (2019).
36. E. Bulgakov and A. Sadreev, Phys. Rev. B **98**, 085301 (2018).
37. X. Gao, B. Zhen, M. Soljačić, H. Chen, and C. W. Hsu, ACS Photonics **6**, 2996 (2019).
38. D. C. Marinica, A. G. Borisov, and S. V. Shabanov, Phys. Rev. Lett. **100**, 183902 (2008).
39. S. A. Maier, *Plasmonics: Fundamentals and Applications* (Springer, 2007).
40. L. J. Sherry, S. H. Chang, G. C. Schatz, R. P. Van Duyne, B. J. Wiley, and Y. Xia, Nano Lett. **5**, 2034 (2005).
41. Y. Shen, J. Zhou, T. Liu, Y. Tao, R. Jiang, M. Liu, G. Xiao, J. Zhu, Z.-K. Zhou, X. Wang, C. Jin, and J. Wang, Nat. Commun. **4**, 2381 (2013).
42. R. Ameling, L. Langguth, M. Hentschel, M. Mesch, P. V. Braun, and H. Giessen, Appl. Phys. Lett. **97**, 253116 (2010).
43. W. Chen, H. Hu, W. Jiang, Y. Xu, S. Zhang, and H. Xu, Chin. Phys. B **27**, 107403 (2018).